

# Comparison of the Photophysical Parameters for Three Perylene Bisimide Derivatives by Single-Molecule Spectroscopy

Erwin Lang,<sup>[a]</sup> Richard Hildner,<sup>[a]</sup> Hanna Engelke,<sup>[a]</sup> Peter Osswald,<sup>[b]</sup> Frank Würthner,<sup>[b]</sup> and Jürgen Köhler\*<sup>[a]</sup>

*Characterization of the photophysical parameters for three perylene bisimide derivatives is presented. We exploited time-resolved and steady-state spectroscopy on both ensembles and single molecules under ambient as well as cryogenic (1.4 K) conditions.*

*The finding is that these chromophores show extraordinary high fluorescence-emission rates, low intersystem crossing yields to the triplet state, and relatively short triplet lifetimes.*

## 1. Introduction

One of the greatest challenges in chemical physics is the exploitation of the features of organic matter for technological applications<sup>[1]</sup> because organic matter offers the opportunity to design novel devices with controlled structures and tailored electronic properties. The various types of model systems that have been intensively investigated include conjugated polymers,<sup>[2–5]</sup> J-aggregates,<sup>[6–9]</sup> and pigment–protein complexes.<sup>[10–14]</sup> In recent years, the perylene bisimides (PBI) have become one of the most useful classes of chromophores, and are frequently used for coloration as car pigments, as sensitizers for organic solar cells, or as laser dyes,<sup>[15–18]</sup> while their extraordinary photostability and high fluorescence quantum yield makes these pigments very interesting for use in fluorescence-based sensors or as markers in biomedical applications.<sup>[19]</sup> Moreover, PBIs bearing phenoxy substituents at the bay positions can be functionalized at the imide and bay phenoxy units to achieve desired optical and electrochemical properties. Hence it is not surprising that these chromophores have played a prominent role in the search for novel functional organic materials in recent years. Indeed highly efficient excitation energy and charge transfer properties have been demonstrated for multi-chromophoric dendrimers,<sup>[20,21]</sup> self-organized metallo-supramolecular molecular squares,<sup>[22–24]</sup> and donor–acceptor dyads<sup>[25–29]</sup> based on these chromophores.

The functional properties of such assemblies are determined by the properties of the electronically excited states of the aggregate, which in turn depend crucially on both the geometric arrangement of the subunits with respect to each other and the properties of the electronically excited states of the molecular building blocks. A significant effect of the twist of PBI chromophores and the mutual orientation of the phenoxy side groups on the photophysics of the immobilized PBI molecules was revealed by single-molecule spectroscopy<sup>[30]</sup> and later confirmed for conformationally rigidified chromophores in solution.<sup>[31]</sup> However, despite the great versatility of the PBI mole-

cules a systematic characterization of their photophysical parameters is still lacking, in particular regarding the role of the triplet state. Given the high fluorescence quantum yield it is expected that the intersystem crossing rate to the triplet manifold is very low, which prevents information about the triplet state from being obtained by conventional spin-resonance techniques. For the triplet state only upper bound estimates for the lifetime ( $< 100 \mu\text{s}$ ) and triplet yield ( $< 10^{-3}$ ) have been deduced from ensemble experiments.<sup>[32]</sup>

Here we exploit single-molecule spectroscopy to compare the photophysical properties of three PBI derivatives, shown schematically in Figure 1 and labeled PBI A, B, and C. They have been chosen for the following reasons: PBI A is one of the best characterized chromophores within the class of tetraphenoxy-bay-substituted perylene bisimides<sup>[21,25,33–37]</sup> and PBI C has been applied as a molecular building block in several self-assembled supramolecular architectures.<sup>[38]</sup> However, recently there is increasing evidence from spectroscopic studies of these and related tetraphenoxy-substituted perylene bisimides that these dyes can exist in two conformational states that exhibit quite different emission properties, that is, fluorescence maxima, excited state lifetime and fluorescence quantum yield.<sup>[36]</sup> According to a previous study on different macrocyclic perylene bisimides<sup>[31]</sup> PBI A and PBI C exist predominantly in a conformation where the phenoxy arms are spread laterally, which leads to absorption and fluorescence maxima at longer wavelengths. In contrast, PBI B was found to be conformation-

[a] Dr. E. Lang, R. Hildner, H. Engelke, Prof. Dr. J. Köhler  
Experimental Physics IV and BIMF  
University of Bayreuth, 95440 Bayreuth (Germany)  
Fax: (+49) 921-55-4002  
E-mail: Juergen.Koehler@uni-bayreuth.de

[b] Dr. P. Osswald, Prof. Dr. F. Würthner  
Institut für Organische Chemie, Universität Würzburg  
97074 Würzburg (Germany)

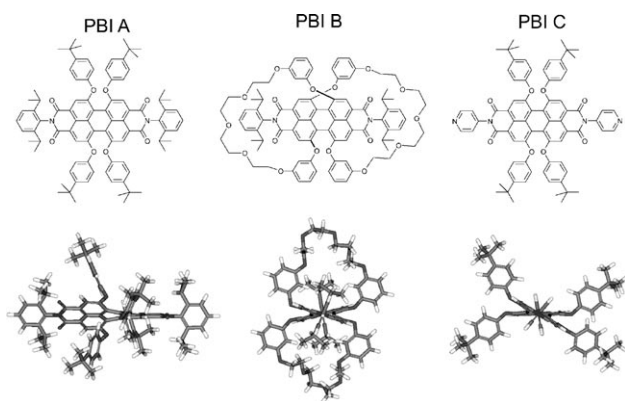


**Figure 1.** Schematic representation of the three perylene bisimide fluorophores termed PBI A, B, and C. The lower part shows the results of molecular-dynamics simulations. PBI A: side view; PBI B and PBI C: view along the axis that connects the nitrogen atoms of the perylene bisimide.

ally restricted towards a conformation with more-perpendicular phenoxy arms; its spectroscopic properties have not yet been elucidated in detail.

Another driving force for this work is the ongoing search for guest–host combinations that are suitable for single-molecule spectroscopy at low temperatures.<sup>[39,40]</sup> Under these conditions the absorption of the individual molecules become extremely narrow and ideally the linewidth is limited only by the finite lifetime of the electronically excited state. This provides a versatile tool to monitor interactions in condensed matter on a truly local scale with high sensitivity since tiny changes in the environment of the probe molecule are sufficient to shift the absorption line by more than its width. Moreover single molecules can be considered unique light sources enabling quantum optical experiments and nanophotonic devices.<sup>[41–45]</sup>

Here we present a detailed study of the photophysical properties of three PBI derivatives at low temperatures. Therefore the chromophores were immobilized in a Shpol'skii matrix of hexadecane, which allowed us to reveal the triplet substate kinetics for the three PBI species. The photophysical properties of PBI C have been investigated by our group previously.<sup>[46,47]</sup> Unfortunately, in that study the calculation of the triplet population and depopulation rates were based erroneously on an improperly normalized autocorrelation function. Here, we find that the triplet yields for all PBI derivatives are very small (intersystem crossing yield about  $10^{-5}$  or smaller) and that the triplet kinetics for PBI A and PBI C is quite similar whereas the triplet population and depopulation rates are even an order of magnitude lower for PBI B. The small intersystem crossing rate is consistent with the observed high fluorescence count rate [up to 930 000 detected counts per second (cps)] for the fully saturated emission rate, which makes these guest–host systems a suitable model system for single-molecule studies at low temperatures.

## Experimental Section

**Sample Preparation:** The PBI A and PBI C derivatives were available from earlier studies<sup>[48]</sup> and PBI B was synthesized as described in

ref. [31]. For the single-molecule experiments, hexadecane was chosen as the host to immobilize the chromophores. It is known that upon fast cooling n-alkanes form a Shpol'skii matrix,<sup>[49]</sup> providing a reasonably well-defined nanoenvironment for the guest molecules. A solution of about  $10^{-10}$  mol L<sup>-1</sup> PBI in hexadecane is prepared by predissolving a tiny speck of the chromophore material in dichloromethane. Next, this mixture is diluted in hexadecane and heated for about 30 min to 60 °C to evaporate residual dichloromethane. Subsequently, a drop of this solution is placed on an LiF substrate and squeezed by a glass cover plate to ensure that the liquid forms a uniform film with a typical thickness of some ten micrometers. To achieve a Shpol'skii matrix the sample was inserted quickly into a precooled (80 K) cryostat. All single-molecule experiments have been carried out at 1.4 K.

For steady-state ensemble spectroscopy the monomers were dissolved in dichloromethane while for time-resolved ensemble spectroscopy the solvent was hexadecane where the monomers were predissolved in dichloromethane.

**Ensemble Spectroscopy:** UV/Vis absorption spectra were taken on a spectrophotometer (Perkin–Elmer Lambda 40P) equipped with a Peltier temperature controller. Fluorescence emission and excitation spectra were recorded on a fluorescence spectrometer (PTI QM4-2003) equipped with a Peltier temperature controller and were corrected against photomultiplier (Hamamatsu R928) and lamp intensity. Room-temperature fluorescence quantum yields were determined in dichloromethane versus *N,N'*-bis(2,6-diisopropylphenyl)-1,6,7,12-tetraphenoxyperylene-3,4:9,10-tetracarboxylic acid bisimide as reference ( $\Phi_{\text{fl}} = 0.96$  in CHCl<sub>3</sub><sup>[33,34]</sup>).

For the time-resolved experiments we used a titanium:sapphire laser system (Tsunami, Spectra-Physics) combined with a pulse picker/frequency doubler (Model 3980, Spectra-Physics) that provided excitation pulses of 1.5 ps (full-width at half-maximum, FWHM). For the room-temperature experiments the excitation light was focused by an achromatic lens (focal length  $f = 100$  mm) into the sample solution. The sample was excited at 450 nm at a repetition rate of 2 MHz. The excitation power was 50–150  $\mu$ W (average) corresponding to 16–50 W (per pulse) or equivalently to an excitation intensity (energy per time-area) of 0.6–2 W cm<sup>-2</sup>. The emission was collected at an angle of 90° and imaged onto the entrance slit of a spectrograph (C5094, Hamamatsu) by two achromatic lenses ( $f = 100$  mm). The spectrograph was equipped with a 100 lines/mm grating providing a spectral resolution of 100 cm<sup>-1</sup>. The spectrally resolved light was then imaged onto the entrance slit of a streak camera system (C5680 Slow Speed Unit, Hamamatsu Photonics), and the resulting streak images were read out by a computer-controlled charge-coupled device (CCD) camera and integrated using the photon counting method. The instrument response function (IRF) of the setup was determined to be 250 ps (FWHM). At low temperature we used the same setup as described below for the single-molecule experiments. The sample was excited at 475 nm at a repetition rate of 8.1 MHz. The excitation power was 0.1–1  $\mu$ W (average) corresponding to 8–80 mW (per pulse) or equivalently to an excitation intensity of 20–200 W cm<sup>-2</sup>. Due to the drastic reduction of the excitation volume and the lower solubility of the PBI derivatives in hexadecane at cryogenic temperatures, the sensitivity of the streak camera system was not sufficient for data acquisition. Therefore we had to employ time-correlated single-photon counting (TCSPC) using a computer-based board (TimeHarp200, PicoQuant). For this method the overall IRF width was 1 ns (FWHM). Analysis of the data with commercial software (FluoFit 3.3, PicoQuant) exploiting deconvolution techniques allowed us to achieve a temporal resolution of about 500 ps.

**Single-Molecule Spectroscopy:** For the single-molecule experiments we used a versatile setup that can be operated either as a confocal or wide-field microscope and that allowed us to vary between different lasers and detectors.<sup>[50]</sup> Changes of the components were accomplished by flipping some of the optical elements into or out of the optical path, as sketched in Figure 2. As the exci-

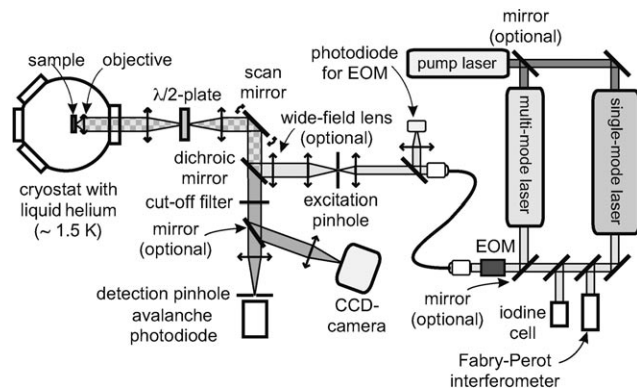


**Figure 2.** Schematic arrangement of the experimental setup.

tation light source we used either a tunable multi-mode dye laser (599, Coherent, spectral bandwidth about 20 GHz) or a tunable single-mode dye laser (699-29, Coherent, spectral bandwidth less than 2 MHz), both operated with Rhodamine 6G and pumped by an Ar-ion laser (Innova 310, Coherent). To obtain a well-defined variation of the wavelength of the multi-mode laser, the intracavity birefringent filter was rotated with a motorized micrometer. For calibration purposes a wavemeter was used and an accuracy and reproducibility of  $1 \text{ cm}^{-1}$  was verified for the laser frequency.

For the single-mode laser an iodine cell in combination with a Fabry-Perot interferometer (Tropel M 240, Coherent, free spectral range 300 MHz) was used to determine spectral positions with an absolute accuracy of  $0.003 \text{ cm}^{-1}$ . After amplitude stabilization to within 1% by an electro-optical modulator the output of one of the lasers was coupled into the homebuilt microscope via a single-mode polarization-conserving fiber. This allows to switch very efficiently between long low-resolution laser scans and short high-resolution laser scans. The excitation and detection paths were separated by a beam splitter, which reflects the laser light towards the cryostat. A  $\lambda/2$  plate allows to rotate the polarization of the incident radiation in increments of  $1.8^\circ$ . In confocal mode the excitation light is focused to a spot size of 410 nm (FWHM) by an objective (either  $\text{NA} = 0.90$ , Microthek or  $\text{NA} = 0.85$ , Halle), immersed in liquid helium. A motorized scan mirror in combination with two telecentric lenses allows precise movement of the focal spot across the sample. In the wide-field mode an additional lens is placed into the excitation path in front of the beam splitter to defocus the excitation light to an area of about  $50 \times 50 \mu\text{m}^2$ . In either case, the fluorescence is collected by the objective and passed through a system of dielectric filters (HQ610 LP, AHF). In confocal mode the emission is focused onto a single-photon counting avalanche photodiode (SPCM-AQR-15, EG&G) and recorded with computer-based multifunctional counter devices (National Instruments). In wide-field mode the fluorescence images are registered with an electron-multiplying CCD camera (DV887DCS-BV, Andor Technology).

To obtain time-resolved information from individual PBI molecules autocorrelation measurements were performed, in which the laser frequency was tuned into resonance with a single-molecule absorption and the signal was accumulated in  $10 \mu\text{s}$  time bins by a

multiscaler (P7882 Dual input Multiscaler, Fast ComTec GmbH). Typical time traces had a duration of about 5 s and were stored separately in computer memory.

**Spatial and Spectral Selection of an Individual Molecule:** The low solubility of the PBI molecules in hexadecane and the concomitant low concentration in the probe excitation volume did not permit the observation of an inhomogeneously broadened ensemble absorption line. Therefore, the selection of an individual PBI molecule in hexadecane requires the simultaneous determination of its accurate spatial and spectral position. The experimental challenge is to find the narrow absorption of an individual PBI molecule of some  $10 \text{ MHz}$  ( $0.002 \text{ cm}^{-1}$ ) linewidth that might be distributed over a spectral range of more than  $100 \text{ cm}^{-1}$ . This task was solved in several steps. First, the setup was operated in wide-field mode and the multi-mode laser was scanned over  $100 \text{ cm}^{-1}$  (scan speed  $7 \text{ cm}^{-1} \text{ s}^{-1}$ ) while typically 500 successive images on the CCD camera are acquired. An individual molecule within the field of view is detected by the occurrence of a bright spot in one of the images, which provides the required spatial information. Since the frame number of the CCD read-out corresponds to the excitation wavelength a low-resolution fluorescence–excitation spectrum can be extracted from the data. Subsequently, the excitation is switched to the single-mode laser and the procedure is repeated while only the part of interest of the low-resolution spectrum is scanned. Hence, a high-resolution fluorescence–excitation spectrum from the molecule is obtained, which yields the necessary spectral information. An example of this protocol is presented in more detail in the appendix. In the last step, the microscope is switched to the confocal mode such that the confocal excitation volume coincides with the spatial position of the molecule under study and emission is detected with the avalanche photodiode, which allows a faster read-out than the CCD camera. Before recording fluorescence–excitation spectra, the polarization of the incident light field was optimized for each molecule with respect to the projection of the molecular transition-dipole moment on the plane normal to the optical axis.

## 2. Results

### Ensemble Spectroscopy

The room-temperature absorption (solid line) and emission spectra (dashed line) of the three PBI derivatives dissolved in dichloromethane are shown in Figure 3. For PBI A (PBI B, PBI C) the absorption spectrum features a broad peak at 585 nm (557 nm, 585 nm) which is accompanied by a shoulder at about 540 nm (520 nm, 540 nm) and a weaker maximum at about 450 nm. The gross shape of the three spectra is very similar and the most obvious distinction between them is a blue shift of the PBI B absorption spectrum of about 28 nm ( $860 \text{ cm}^{-1}$ ) with respect to the absorption spectra of the other two derivatives. The maxima at 585 nm for PBI A and PBI C, and at 557 nm for PBI B correspond to the electronic  $S_1 \leftarrow S_0$ , highest occupied molecular orbital to lowest unoccupied molecular orbital (HOMO–LUMO), transition and the accompanying shoulder corresponds to intramolecular vibrational states coupled to the electronic  $S_1$  state. The maximum at about 450 nm is ascribed to transitions involving higher electronic states. The emission spectra of the three PBI derivatives feature a Stokes shift of about 30 nm ( $870 \text{ cm}^{-1}$ ) and their shape close-

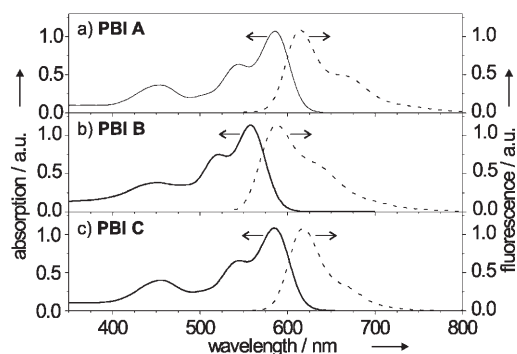


**Figure 3.** Room-temperature absorption (solid line) and emission (dashed line) spectra from: a) PBI A, b) PBI B, and c) PBI C dissolved in dichloromethane. The concentrations of the solutions were  $2 \cdot 10^{-5}$  M for PBI A,  $2.4 \cdot 10^{-5}$  M for PBI B, and  $3.5 \cdot 10^{-5}$  M for PBI C. For better comparison all spectra have been normalized.

ly resembles the mirror image of the part of the absorption spectrum related to the lowest electronic transition.

For the time-resolved ensemble experiments the PBI derivatives were dissolved in hexadecane to allow for a comparison with the single-molecule data. At room temperature we found  $(5.8 \pm 0.2)$  ns,  $(6.0 \pm 0.2)$  ns, and  $(5.9 \pm 0.2)$  ns for the fluorescence lifetimes of PBI A, B, and C, respectively, using the streak camera technique. At cryogenic temperatures (1.4 K) we were not able to observe an ensemble absorption spectrum due to the low solubility of PBI in hexadecane and the concomitant small number of PBI molecules present in the excitation volume. Therefore we had to employ time-correlated single-photon counting to determine the (small) ensemble fluorescence lifetimes and found  $(6.0 \pm 0.5)$  ns for PBI A, and  $(5.3 \pm 0.5)$  ns for PBI B, respectively. For PBI C the number of chromophores in the excitation volume was too small to allow the determination of the low-temperature fluorescence lifetime with reasonable accuracy.

### Single-Molecule Spectroscopy

#### Fluorescence–Excitation Spectroscopy

At low temperatures, single PBI molecules could be excited between  $16550 \text{ cm}^{-1}$  (604 nm) and  $16700 \text{ cm}^{-1}$  (599 nm) for PBI A and PBI C, and between  $17200 \text{ cm}^{-1}$  (581 nm) and  $17600 \text{ cm}^{-1}$  (568 nm) for PBI B. The value of  $17600 \text{ cm}^{-1}$  for PBI B is determined by the limited scan range of the laser. For all species we observed that about 30–40% of the molecules were subjected to light-induced spectral diffusion. The other molecules were spectrally stable, at least up to moderate excitation intensities. As an example of these molecules we show in Figure 4 two fluorescence–excitation spectra recorded for low and high excitation intensities for each species. For PBI A a narrow line with a width of 29 MHz (FWHM) and a maximum photon count rate of about 2000 counts per second (cps) is observed at low excitation intensity ( $0.22 \text{ W cm}^{-2}$ ), Figure 4a. As the excitation intensity increased to  $550 \text{ W cm}^{-2}$  the background-corrected maximum photon count rate grew to 42000 cps and the linewidth increased to 339 MHz, Figure 4b.

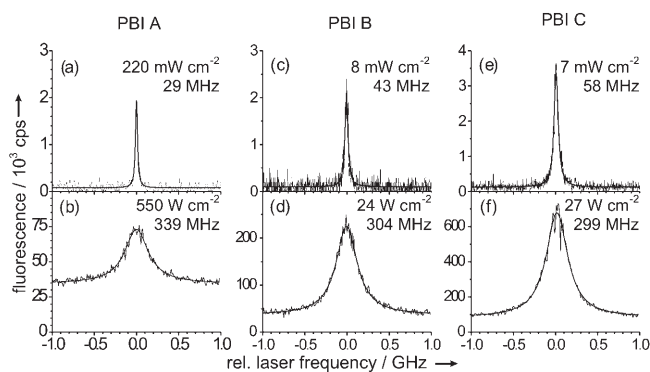


**Figure 4.** Fluorescence–excitation spectra of an individual molecule of PBI A (a,b), PBI B (c,d) and PBI C (e,f) in hexadecane at 1.4 K. The peak of the absorptions corresponds to  $16664.080 \text{ cm}^{-1}$  (PBI A),  $17467.308 \text{ cm}^{-1}$  (PBI B) and  $16603.667 \text{ cm}^{-1}$  (PBI C). The fluorescence intensity is given in  $10^3$  counts per second (cps). a) [b]) Average of 10 individual spectra of PBI A recorded at a speed of  $10 \text{ GHz s}^{-1}$  for low [high] excitation intensity of  $220 \text{ mW cm}^{-2}$  [ $550 \text{ W cm}^{-2}$ ]. c) [d]) Average of 20(3) individual spectra of PBI B recorded at a speed of  $2 \text{ GHz s}^{-1}$  [ $10 \text{ GHz s}^{-1}$ ] for low [high] excitation intensity of  $8 \text{ mW cm}^{-2}$  [ $24 \text{ W cm}^{-2}$ ]. e) [f]) Average of 20(3) individual spectra of PBI C recorded at a speed of  $2 \text{ GHz s}^{-1}$  [ $10 \text{ GHz s}^{-1}$ ] for low [high] excitation intensity of  $7 \text{ mW cm}^{-2}$  [ $27 \text{ W cm}^{-2}$ ]. The solid lines correspond to Lorentzians with a width (FWHM) of 29 MHz (a), 339 MHz (b), 43 MHz (c), 304 MHz (d), 58 MHz (e) and 299 MHz (f) fitted to the data.

For PBI B we observed a linewidth (peak count rate) of 43 MHz (2500 cps) at low excitation intensity ( $0.008 \text{ W cm}^{-2}$ ) and 304 MHz (200 000 cps) at higher excitation intensities ( $24 \text{ W cm}^{-2}$ ), Figures 4c and 4d, and for PBI C the respective numbers are 58 MHz (3500 cps) at  $0.007 \text{ W cm}^{-2}$  and 299 MHz (630 000 cps) at  $27 \text{ W cm}^{-2}$ , Figures 4e and 4f. Moreover, the high-intensity spectral profile of PBI C shows a few dips where the fluorescence count rate drops, which we attribute to intersystem crossing from the excited singlet state to the triplet manifold as will be discussed later. All observed lineshapes can be described by a Lorentzian profile.

To study the dependence of the linewidth on the excitation conditions in more detail we recorded fluorescence–excitation spectra as a function of the excitation intensity. In Figure 5 we display from top to bottom the peak fluorescence count rate versus the excitation intensity, the spectral linewidth versus the excitation intensity, and the peak fluorescence count rate versus the linewidth for PBI A (left), PBI B (center), and PBI C (right). The individual molecules are the same as those shown in Figure 4. At low excitation intensity the peak fluorescence count rate increases linearly with increasing intensity and saturates at high excitation levels. The observed linewidth  $\Gamma$  shows little variation at low excitation intensity and grows rapidly with increasing excitation rate. These findings reflect the well-known saturation and power broadening behavior of an optical transition, which can be described by Equations (1)<sup>[51]</sup> and (2),

$$C(I) = D \cdot R(I) = D \cdot R_{\infty} \cdot \frac{I}{I_s} \cdot \left(1 + \frac{I}{I_s}\right)^{-1} = C_{\infty} \cdot \frac{I}{I_s} \cdot \left(1 + \frac{I}{I_s}\right)^{-1} \quad (1)$$

$$\Gamma(I) = \Gamma_0 \sqrt{1 + \frac{I}{I_s}} \quad (2)$$

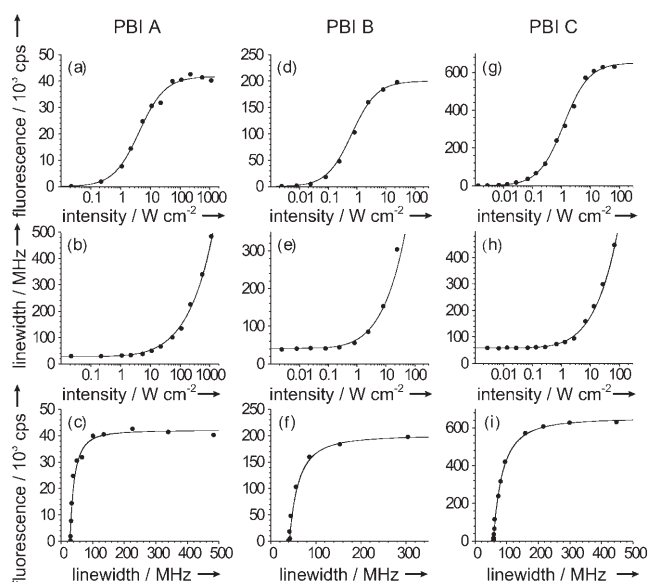


**Figure 5.** Saturation behavior for the same molecules shown in Figure 4. a) Fluorescence intensity and b) linewidth for an individual PBI A molecule as a function of the excitation intensity. c) The same data plotted as fluorescence intensity versus the linewidth. The solid lines are fits of the data according to the usual saturation behavior equations and yield  $I_s = 4.0 \text{ W cm}^{-2}$  for the saturation intensity,  $\Gamma_0 = 28 \text{ MHz}$  for the homogeneous linewidth, and  $C_\infty = 42000 \text{ cps}$  for the fully saturated count rate. In (d–f) the data are plotted in a similar way for the PBI B molecule. The fits yield  $I_s = 0.65 \text{ W cm}^{-2}$  for the saturation intensity,  $\Gamma_0 = 41 \text{ MHz}$  for the homogeneous linewidth, and  $C_\infty = 200000 \text{ cps}$  for the fully saturated count rate. In (g–i) the corresponding data are plotted for the PBI C molecule. The fits yield  $I_s = 1.2 \text{ W cm}^{-2}$ ,  $\Gamma_0 = 58 \text{ MHz}$ , and  $C_\infty = 650000 \text{ cps}$ .

where  $C(I)$  denotes the peak fluorescence count rate,  $C_\infty = D \cdot R_\infty$  is the fully saturated count rate,  $R(I)$  is the rate of emitted photons,  $R_\infty$  is the fully saturated emission rate,  $D$  is the detection efficiency of the optical setup,  $I$  is the excitation intensity,  $I_s$  is the saturation intensity,  $\Gamma(I)$  is the observed linewidth of the transition, and  $\Gamma_0$  is the homogeneous linewidth of the transition. Combining Equations (1) and (2) allows the elimination of the excitation intensity, which yields Equation (3):

$$C(\Gamma) = C_\infty \left( 1 - \left( \frac{\Gamma_0}{\Gamma} \right)^2 \right) \quad (3)$$

Fitting the data presented in Figure 5 simultaneously to Equations (1), (2), and (3) yields for PBI A (PBI B; PBI C) a saturation intensity of  $I_s = 4 \text{ W cm}^{-2}$  ( $0.65 \text{ W cm}^{-2}$ ;  $1.2 \text{ W cm}^{-2}$ ), a fully saturated count rate of  $C_\infty = 42000 \text{ cps}$  ( $200000 \text{ cps}$ ;  $650000 \text{ cps}$ ), and a homogeneous linewidth of  $\Gamma_0 = 28 \text{ MHz}$  ( $41 \text{ MHz}$ ;  $58 \text{ MHz}$ ), respectively. The fits are indicated in Figure 5 by the solid lines and are in good agreement with the experimental data. Similar observations were made for 15 PBI A, 11 PBI B, and 16 PBI C molecules in total. Even within each species the obtained parameters showed considerable variations. For example for PBI A the measured saturation intensity ranges from 1 to  $90 \text{ W cm}^{-2}$  (average  $12 \text{ W cm}^{-2}$ ), the fully saturated count rate varies between 16000 and 690000 cps (average 230000 cps), and the homogeneous linewidths covers the range 25–57 MHz (average 38 MHz). A comparable spread in

these parameters is also observed for the other two PBI derivatives, as summarized in Table 1. For each species the distribution of the measured homogeneous linewidths is shown in

**Table 1.** Minimum, maximum and average values (in parentheses) of the saturation intensity, the homogeneous linewidth and the fully saturated count rate for 15 PBI A, 11 PBI B, and 16 PBI C molecules.

	$I_s [\text{W cm}^{-2}]$	$\Gamma_0 [\text{MHz}]$	$C_\infty [\text{s}^{-1}]$
PBI A	1.0–90 (12)	25–57 (38)	16000–690000 (230000)
PBI B	0.4–2.7 (1.1)	27–44 (37)	30000–270000 (100000)
PBI C	0.3–23 (4.7)	29–62 (53)	107000–930000 (490000)

Figure 6. In contrast to the linewidth distributions for PBI B and PBI C, which are centered around a mean of 40 MHz and 55 MHz, respectively, nine PBI A molecules feature a linewidth

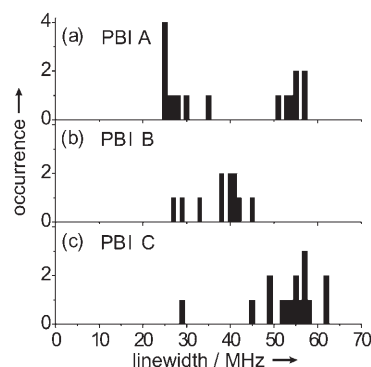


**Figure 6.** Distributions of the homogeneous linewidths for PBI A (a), PBI B (b) and PBI C (c).

between 25 and 35 MHz, whereas six PBI A molecules feature a linewidth between 50 and 57 MHz, which makes the PBI A linewidth distribution bimodal.

### Autocorrelation

A few molecules did not show spectral diffusion even under conditions of high excitation intensity. For these molecules we recorded the flux of emitted photons as a function of excitation intensity and calculated the fluorescence–autocorrelation function according to Equation (4):

$$g^{(2)}(\tau) = \frac{\langle I(t)I(t+\tau) \rangle}{\langle I(t) \rangle^2} \quad (4)$$

Here the brackets denote an average over time and  $I(t)$  and  $I(t+\tau)$  denote the intensity  $I$  at time  $t$  and  $(t+\tau)$ , respectively. An example for each PBI derivative is shown in Figure 7. The autocorrelation functions were recorded at 1.4 K for excitation intensities of  $14 \text{ W cm}^{-2}$  (PBI A),  $8 \text{ W cm}^{-2}$  (PBI B), and  $13 \text{ W cm}^{-2}$  (PBI C). In all cases we failed to explain the recorded

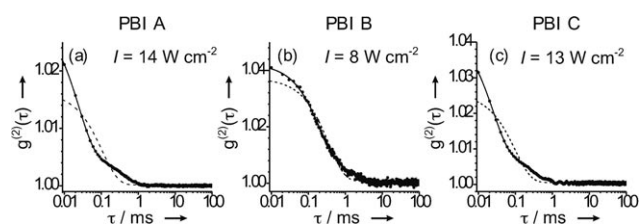


**Figure 7.** Second-order autocorrelation function of the fluorescence intensity of a single PBI A (a), PBI B (b) and PBI C (c) molecule in hexadecane at 1.4 K. The PBI A (PBI B, PBI C) molecule has been excited resonantly at  $16630.875\text{ cm}^{-1}$  ( $17467.308\text{ cm}^{-1}$ ,  $16620.335\text{ cm}^{-1}$ ) with an excitation intensity of  $14\text{ W cm}^{-2}$  ( $8.0\text{ W cm}^{-2}$ ,  $13\text{ W cm}^{-2}$ ). The dashed lines correspond to a single exponential fit with a decay time of  $100\text{ }\mu\text{s}$  ( $360\text{ }\mu\text{s}$ ,  $100\text{ }\mu\text{s}$ ). The solid line corresponds to a bi-exponential decay with decay times of  $24\text{ }\mu\text{s}$  and  $360\text{ }\mu\text{s}$  ( $180\text{ }\mu\text{s}$  and  $1.2\text{ ms}$ ,  $20\text{ }\mu\text{s}$  and  $300\text{ }\mu\text{s}$ ).

autocorrelation functions by a single exponential fit, as shown by the dashed lines in Figure 7. Taking a bi-exponential fit function [Eq. (5)]:

$$g^{(2)}(\tau) = 1 + C_1 \exp(-\lambda_1 \tau) + C_2 \exp(-\lambda_2 \tau) \quad (5)$$

with decay rates  $\lambda_1$ ,  $\lambda_2$  and contrasts  $C_1$ ,  $C_2$  into account yields nearly perfect agreement with the data, as testified by the solid lines in Figure 7 and as summarized in Table 2.

	Contrast $C_1$	Contrast $C_2$	Decay rate $\lambda_1$ [ $\text{s}^{-1}$ ]	Decay rate $\lambda_2$ [ $\text{s}^{-1}$ ]
PBI A	0.23	0.06	41 700	2800
PBI B	0.032	0.010	5600	810
PBI C	0.034	0.09	50 000	3300

### 3. Discussion

#### Fluorescence

The large spreads in the saturation intensities and maximum count rates observed for PBI molecules of the same species are attributed to variations in the orientations of the transition-dipole moments of the molecules with respect to the polarization of the electric field vector of the excitation light and to the fact that the detection efficiency depends on the orientation of the molecule. Upon lowering the temperature we observe for PBI A a slight increase in the fluorescence lifetime whereas for PBI B we even observe a decrease of the fluorescence lifetime. The TCSPC technique inherently underestimates values for the lifetimes if the number of detected photons is not sufficiently low. However, for PBI B the observed discrep-

ancy between the room-temperature and low-temperature fluorescence lifetimes appears too large to result exclusively from this experimental shortcoming. An independent piece of information about the low-temperature fluorescence lifetime can be obtained from the homogeneous linewidth,  $\Gamma_0$ , of the optical transition. This linewidth is related to the fluorescence lifetime via Equation (6):

$$\Gamma_0 = \frac{1}{\pi T_2} = \frac{1}{2\pi T_1} + \frac{1}{\pi T_2^*} \quad (6)$$

where  $T_2$  refers to the total dephasing time,  $T_1$  to the fluorescence lifetime, and  $T_2^*$  to the pure dephasing time. However, the experimentally observed linewidth might also reflect contributions from spectral diffusion that occurs while the laser scans through the absorption. Given the flexible side chains attached to the bay positions, in particular for the PBI C derivative, such contributions are not unlikely and have been observed previously, for example for tetra-tert-butylterrylene (TBT) in polymethylmethacrylate (PMMA) by photon echo spectroscopy.<sup>[52]</sup> Consequently, the smallest values that have been observed for the linewidth can serve only as an estimate for the lower bound to the low-temperature lifetime of the PBI derivatives in hexadecane. These considerations yield as lower limits  $6.4\text{ ns}$  for PBI A,  $5.9\text{ ns}$  for PBI B, and  $5.5\text{ ns}$  for PBI C. For better comparison the fluorescence lifetimes (and boundaries) obtained under various experimental conditions are summarized in Table 3. Taking into account the shortcomings of the TCSPC technique, the agreement between the results of the two low-temperature experiments is reasonable.

The comparison of fluorescence lifetimes measured at room temperature and at cryogenic temperatures may be hampered by conformational changes of the PBI molecules upon incorporation into the host matrix.<sup>[30]</sup> Investigations on a tetra-phenoxy perylene derivative that closely resembles the PBI A molecule studied here showed the influence of the free volume of different polymer matrices on the fluorescence lifetime.<sup>[36]</sup> These authors found a bimodal distribution for the fluorescence lifetime peaking at  $6.2\text{ ns}$  and  $3.2\text{ ns}$ , which corresponded to a twisted and a more planar conformation of the perylene molecule, respectively. If we neglect spectral diffusion and pure dephasing processes ( $T_2^*$ ) these numbers correspond to homogeneous linewidths of  $25\text{ MHz}$  and  $50\text{ MHz}$ , respectively, consistent with the bimodal linewidth distribution that we observed for PBI A. Cooling down from room temperature to cryogenic tempera-

**Table 3.** Summary of the fluorescence lifetimes obtained for various experimental conditions. The single-molecule value in parenthesis for PBI A corresponds to the lower boundary estimated from the smallest linewidth of the second peak in the linewidth distribution.

	Ensemble	Single molecule
	room temperature	low temperature
	streak camera	TCSPC
	$\tau$ [ns]	$\tau$ [ns]
PBI A	$5.8 \pm 0.3$	$6.0 \pm 0.5$
PBI B	$6.0 \pm 0.3$	$5.3 \pm 0.5$
PBI C	$5.9 \pm 0.3$	–
		lower bound from linewidth
		$\tau$ [ns]
		$6.4$ (3.2)
		5.9
		5.5

tures clearly affects the hexadecane solvent cage that surrounds the PBI molecules. Hence it appears possible that this affects the conformations of the PBI molecules as well. If so, a comparison of the fluorescence lifetimes at ambient and cryogenic temperatures is pointless.

### Triplet Kinetics

Evaluation of the autocorrelation experiments allows us to obtain information about the triplet kinetics of the PBI derivatives. The decay of the autocorrelation function on a 100  $\mu$ s timescale is known as photon bunching<sup>[53]</sup> and results from intersystem crossing (ISC) of the molecule to the triplet state, preventing its participation in the  $S_1$ - $S_0$  excitation-emission cycles. Generally, at low temperatures spin-lattice relaxation between the triplet sublevels can be neglected and one would expect three distinct exponential components in the autocorrelation function because the triplet substates feature different population and depopulation kinetics. In analogy to studies on pentacene,<sup>[54,55]</sup> terrylene,<sup>[56]</sup> terrylenediimide (TDI),<sup>[57]</sup> and dibenzanthanthrene (DBATT)<sup>[58]</sup> in various matrices we interpret the observation of only two distinct components in the decay of the autocorrelations for PBI A, B, and C to result from three triplet sublevels, two of which are too close in population/depopulation kinetics to be resolved experimentally. To derive the population and depopulation rates we approximate the triplet state by two effective triplet sublevels, denoted *fast* and *slow*, and follow the formalism in ref. [58]. Briefly, an effective four-level system including a singlet ground state, a singlet excited state and two triplet sublevels is analyzed in terms of the optical Bloch equations. Under the assumption that the rates involving the triplet state are much smaller than the coherence and population decay of the excited singlet state the authors show that the autocorrelation function is described by a sum of two exponentials as given in Equation (5). For the observables of the autocorrelation function this leads to Equations (7a) and (7b),

$$\lambda_{1,2} = \frac{1}{2}(p_{\text{fast}} + k_{\text{fast}} + p_{\text{slow}} + k_{\text{slow}} \pm S) \quad (7a)$$

$$C_{1,2} = \pm \frac{[(p_{\text{fast}} + p_{\text{slow}} \pm S)(p_{\text{fast}}k_{\text{slow}} + p_{\text{slow}}k_{\text{fast}})] + (k_{\text{slow}} - k_{\text{fast}})(p_{\text{slow}}k_{\text{fast}} - p_{\text{fast}}k_{\text{slow}})}{2k_{\text{fast}}k_{\text{slow}}S} \quad (7b)$$

with  $S$  defined by Equation (8),

$$S = \sqrt{(p_{\text{fast}} + k_{\text{fast}} - p_{\text{slow}} - k_{\text{slow}})^2 + 4k_{\text{fast}}k_{\text{slow}}} \quad (8)$$

where  $k_{\text{slow}}$  and  $k_{\text{fast}}$  refer to the triplet depopulation rates and  $p_{\text{slow}}$  and  $p_{\text{fast}}$  to the effective triplet population rates. These are related to the molecular intersystem crossing (ISC) rates  $P_{\text{slow}}$  and  $P_{\text{fast}}$  by Equations (9a) and (9b):

$$p_{\text{fast}} = FP_{\text{fast}} \quad (9a)$$

$$p_{\text{slow}} = FP_{\text{slow}} \quad (9b)$$

with the  $F$  given by Equation (10):

$$F = \left(2 + \frac{I}{I_s} \left(2 + \sum_i \frac{P_i}{K_i}\right)\right)^{-1} \quad (10)$$

For background correction of the contrast factors we used Equation (11),<sup>[59]</sup>

$$C_{1,2}^{(\text{corr})} = C_{1,2}^{(\text{meas})} \left(1 + \frac{\langle b \rangle}{\langle s \rangle}\right)^2 \quad (11)$$

where  $\langle b \rangle$  and  $\langle s \rangle$  correspond to the average contributions to the measured intensity of the background and the signal, respectively. Figure 8 shows the decay rates  $\lambda_{1,2}$  and the back-

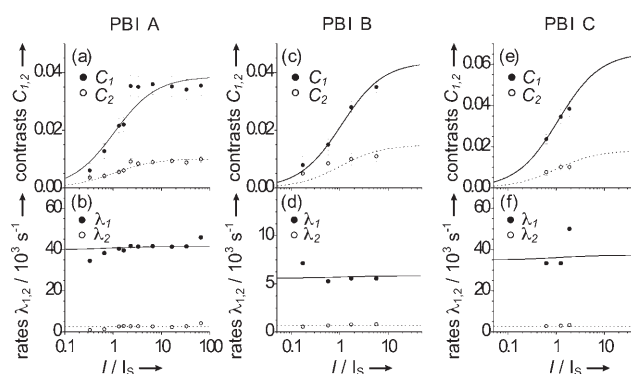


**Figure 8.** Background-corrected contrasts and decay rates of the autocorrelation function of a single PBI molecule in hexadecane at 1.4 K as a function of the excitation intensity: a,b) for PBI A, c,d) for PBI B, and e,f) for PBI C. The solid and dashed lines are fits according to the formalism given in the text. The fitting parameters are  $P_{\text{fast}} = 3050 \text{ s}^{-1}$ ,  $P_{\text{slow}} = 55 \text{ s}^{-1}$ ,  $k_{\text{fast}} = 40000 \text{ s}^{-1}$ ,  $k_{\text{slow}} = 2600 \text{ s}^{-1}$  for PBI A,  $P_{\text{fast}} = 480 \text{ s}^{-1}$ ,  $P_{\text{slow}} = 22 \text{ s}^{-1}$ ,  $k_{\text{fast}} = 5600 \text{ s}^{-1}$ ,  $k_{\text{slow}} = 700 \text{ s}^{-1}$  for PBI B and  $P_{\text{fast}} = 4500 \text{ s}^{-1}$ ,  $P_{\text{slow}} = 110 \text{ s}^{-1}$ ,  $k_{\text{fast}} = 35000 \text{ s}^{-1}$ ,  $k_{\text{slow}} = 2800 \text{ s}^{-1}$  for PBI C.

ground-corrected contrast factors  $C_{1,2}^{(\text{corr})}$  for a single PBI A (PBI B, PBI C) molecule as a function of excitation intensity. For better comparison the excitation intensity is given in units of the saturation intensity, which is  $4.1 \text{ W cm}^{-2}$  ( $0.77 \text{ W cm}^{-2}$ ,  $1.6 \text{ W cm}^{-2}$ ) for this molecule. While the decay rates depend only weakly on the excitation intensity the contrast factors show a clear increase for higher excitation rates. Unfortunately, we were not able to record the autocorrelation function for a single PBI B (PBI C) molecule at more than four (three) distinct excitation intensities. At higher excitation rates irreversible spectral jumps of the absorption occurred, resulting in a loss of the molecule for further experiments. Therefore, we fitted for each molecule the full data simultaneously by a single parameter set according to the formalism discussed above. The results of the fits are shown as solid lines in Figure 8 and are in reasonable agreement with the experimental data. From these fits we obtain the transition rates to and from the triplet sub-

vels with an accuracy of  $\pm 20\%$ . Once the triplet kinetics is determined, we can calculate the fully saturated emission rate  $R_\infty$  according to Equation (12),<sup>[60]</sup>

$$R_\infty = \frac{k}{2\left(1 + \frac{1}{2} \frac{k_{\text{ISC}}}{k_T}\right)} = \frac{k}{2\alpha} \quad (12)$$

where  $k$  is the fluorescence decay rate, and  $\alpha$  is given by Equation (13):

$$\alpha = \left(1 + \frac{1}{2} \frac{k_{\text{ISC}}}{k_T}\right) \quad (13)$$

Table 4 summarizes the photophysical parameters deduced from these data.

The relative steady-state populations of the fast and slow triplet sublevel are very similar, that is,  $n_{\text{fast}} > 70\%$  and  $n_{\text{slow}} < 30\%$ , for the three PBI derivatives. In contrast to this finding, the triplet population and depopulation rates for PBI A and PBI C are about the same, whereas for PBI B these rates are about an order of magnitude smaller. A similar statement holds for the effective triplet lifetimes, that is, about 30  $\mu\text{s}$  for PBI A and PBI C, and 230  $\mu\text{s}$  for PBI B. Since the optical spectra of PBI A and PBI C show a significant red shift with respect to that of PBI B it is very likely that for PBI A and PBI C the energy difference between the electronic ground state and the lowest excited triplet state is also smaller than that of PBI B. Based on this conjecture the differences in the triplet lifetimes of the three PBI derivatives are in qualitative agreement with the energy-gap law,<sup>[61]</sup> which states that a red shift of the triplet state leads to higher Franck–Condon factors for nonradiative relaxation and therefore to shorter triplet lifetimes.

In general the triplet quantum yields obtained for the three PBI derivatives are extremely small and comparable to those reported in the literature for the planar aromatic molecules

**Table 5.** Comparison of the triplet yields, intersystem crossing rates and triplet decay rates for various guest–host systems studied with single-molecule spectroscopy.

Guest/host	$\Phi_T$	$k_{\text{ISC}} [\text{s}^{-1}]$	$k_T [\text{s}^{-1}]$	Reference
terrylene/ <i>p</i> -terphenyl	$6 \cdot 10^{-6}$	$10^3$	$10^3$	[62]
	$2 \cdot 10^{-6}$	$5 \cdot 10^2$	$1.6 \cdot 10^3$	[56]
terrylenediimide/hexadecane	$2 \cdot 10^{-5}$	$\sim 10^3$	$10^3\text{--}10^4$	[57]
DBATT/hexadecane	$10^{-5}$	$1.3 \cdot 10^3$	$5.2 \cdot 10^3$	[58]
DBATT/naphthalene	$4 \cdot 10^{-6}$	$5 \cdot 10^2$	$6.3 \cdot 10^3$	[63]
PBI A/hexadecane	$2 \cdot 10^{-5}$	$3.1 \cdot 10^3$	$4 \cdot 10^4$	[this work]
PBI B/hexadecane	$3 \cdot 10^{-6}$	$5 \cdot 10^2$	$6.3 \cdot 10^3$	[this work]
PBI C/hexadecane	$3 \cdot 10^{-5}$	$4.6 \cdot 10^3$	$3.8 \cdot 10^4$	[this work]

DBATT, Terrylene, and TDI in various matrices.<sup>[56–58,62,63]</sup> Table 5 gives an overview of the triplet quantum yields, the intersystem crossing rates, and the triplet decay rates for the various hydrocarbon molecules and compares these data with the results obtained for the PBI derivatives in the present study. Intersystem crossing (ISC) is caused by spin–orbit coupling (SOC), which mixes singlet and triplet states at a transition rate given by Fermi's golden rule [Eq. (14)],

$$k_{\text{ISC}} = \frac{2\pi}{\hbar} |\langle S_1 | H_{\text{SOC}} | T_n^{(k)} \rangle|^2 \rho_T(E_{S_1}) \quad (14)$$

where  $H_{\text{SOC}}$  represents the SOC Hamiltonian,  $T_n^{(k)}$  is a continuum of (vibronic) levels in the triplet manifold, and  $\rho_T(E_{S_1})$  is the density of levels in the triplet manifold that are isoenergetic with  $S_1$ . The intersystem crossing rate is governed by several contributions and in general one can distinguish electronic SOC, Herzberg–Teller vibronically induced SOC (HT-SOC), and vibronically induced SOC by terms that are commonly neglected in the Born–Oppenheimer approximation (non-BO-SOC).<sup>[64–68]</sup> Due to the lack of heavy atoms in hydrocarbons the contribution from electronic SOC to intersystem crossing is very small or even vanishes for molecules with inversion symmetry.<sup>[64,65]</sup> The other two terms are vibronically induced SOC and contribute non-vanishing terms for polyatomic molecules, and the relative magnitude of the contributions from HT-SOC and non-BO-SOC to the ISC with respect to each other may vary from system to system. Commonly, HT-SOC is primarily induced by in-plane vibrations and leads mainly to  $\pi$ – $\pi$  coupling whereas non-BO-SOC is dominated by out-of-plane terms, which favor  $\sigma$ – $\pi$  coupling. In particular deviations from planarity, which lead to  $\sigma$ – $\pi$  orbital mixing, result in an enhancement of the ISC rate by vibrationally induced SOC. This is generally in line with the finding that for PBI B the triplet population and depopulation rates are about an order of mag-

relative magnitude of the contributions from HT-SOC and non-BO-SOC to the ISC with respect to each other may vary from system to system. Commonly, HT-SOC is primarily induced by in-plane vibrations and leads mainly to  $\pi$ – $\pi$  coupling whereas non-BO-SOC is dominated by out-of-plane terms, which favor  $\sigma$ – $\pi$  coupling. In particular deviations from planarity, which lead to  $\sigma$ – $\pi$  orbital mixing, result in an enhancement of the ISC rate by vibrationally induced SOC. This is generally in line with the finding that for PBI B the triplet population and depopulation rates are about an order of mag-

**Table 4.** Photophysical parameters for the three PBI derivatives.

	PBI A	PBI B	PBI C
fluorescence decay rate [ $\text{s}^{-1}$ ] (room-temperature ensemble)	$1.7 \cdot 10^8$	$1.7 \cdot 10^8$	$1.7 \cdot 10^8$
fluorescence decay rate [ $\text{s}^{-1}$ ] (low-temperature ensemble)	$1.7 \cdot 10^8$	$1.9 \cdot 10^8$	–
fluorescence decay rate [ $\text{s}^{-1}$ ] (low-temperature upper bounds from single-molecule linewidths)	$1.6 \cdot 10^8$ ( $3.1 \cdot 10^8$ )	$1.7 \cdot 10^8$	$1.8 \cdot 10^8$
triplet population rate [ $\text{s}^{-1}$ ]	3100	500	4600
fractional triplet yield	fast: 0.98 slow: 0.02	fast: 0.96 slow: 0.04	fast: 0.98 slow: 0.02
triplet quantum yields $\Phi_T$	$2 \cdot 10^{-5}$	$3 \cdot 10^{-6}$	$3 \cdot 10^{-5}$
triplet decay rate [ $\text{s}^{-1}$ ]	fast: 40 000 slow: 2600	fast: 5600 slow: 700	fast: 35 000 slow: 2800
relative steady-state population	fast: 0.78 slow: 0.22	fast: 0.73 slow: 0.27	fast: 0.77 slow: 0.23
population-weighted triplet lifetime [ $\mu\text{s}$ ]	30	230	36
$\alpha$	1.049	1.058	1.082
fully saturated emission rate $R_\infty$ [ $\text{s}^{-1}$ ]	$7.6 \cdot 10^7$	$8.0 \cdot 10^7$	$8.3 \cdot 10^7$
fully saturated detection rate $C_\infty$ [ $\text{s}^{-1}$ ]	$5.7 \cdot 10^5$	$2.0 \cdot 10^5$	$9.3 \cdot 10^5$

nitude lower than those of PBI A and PBI C, because the conformational freedom of PBI B is more restricted due to the bridged architecture. Nevertheless, it is very surprising that the absolute figures that we found for the triplet quantum yields of the PBI derivatives are as low as  $\sim 10^{-5}$ – $10^{-6}$ , because these molecules deviate significantly from planarity due to steric hindrance of the phenoxy groups at the bay positions. More-detailed statements require an in-depth quantum chemical computation of the SOC matrix elements and we hope that these findings might stimulate further research in this field.

## Conclusions

We studied the photophysical parameters of three PBI derivatives embedded in hexadecane at low temperatures. The chromophores feature narrow zero-phonon lines (linewidths about 30–60 MHz), very high fluorescence emission rates (up to 930 000 detected photons per second for the fully saturated count rate), low intersystem crossing yields (about  $10^{-5}$  or lower), short triplet lifetimes (about 30–230  $\mu$ s), and reasonable photostability with respect to light-induced spectral diffusion. Given these parameters and the relatively simple preparation protocol for the host matrix, which avoids sophisticated crystals growth, this guest–host combination provides a favorable model system for low-temperature single-molecule spectroscopy.

## Appendix

A comparison of the spectroscopy of the same PBI C molecule with the two different lasers as excitation light sources is shown in Figure 9. The top part of the figure displays the fluorescence–excitation spectrum obtained with the multi-mode

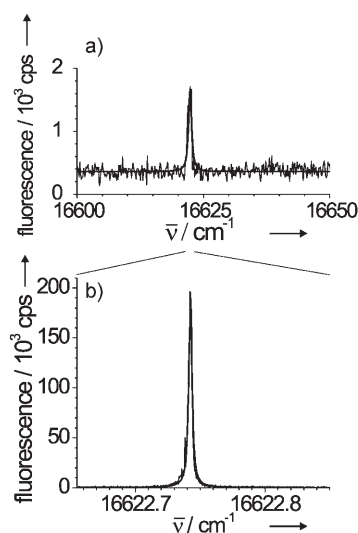


**Figure 9.** Fluorescence–excitation spectra of an individual PBI C molecule in hexadecane at 1.4 K recorded in confocal mode: a) with the multi-mode, and b) with the single-mode laser. The solid lines are Lorentzians with a line-width (FWHM) of a) 21 GHz and b) 87 MHz fitted to the data. For both measurements the excitation intensity was  $0.24 \text{ W cm}^{-2}$ . The saturation intensity for this particular molecule was determined to  $0.27 \text{ W cm}^{-2}$ .

laser whereas the bottom part shows the corresponding data obtained with the single-mode laser. The excitation intensity is  $0.24 \text{ W cm}^{-2}$  for both spectra and the saturation intensity for this particular molecule has been determined to  $I_s = 0.27 \text{ W cm}^{-2}$ . The observed discrepancy in the peak fluorescence count rates between broadband excitation (1350 cps) and narrowband excitation (195 000 cps) can be understood if the effective excitation intensity that excites the molecule is considered. For this example the width,  $\Gamma$ , of the molecular absorption is 87 MHz, that is, broad with respect to the spectral bandwidth of the single-mode laser. Thus, for narrowband excitation the effective excitation intensity,  $I_{\text{eff}}^{(\text{nb})}$ , corresponds to the  $0.24 \text{ W cm}^{-2}$  incident onto the sample. In contrast, for broadband excitation the spectral bandwidth of the laser is  $\Delta\nu_L = 20 \text{ GHz}$ . In simple words, most of the photons that hit the sample are not in resonance with the molecular absorption. An estimate for the effective excitation intensity for broadband excitation  $I_{\text{eff}}^{(\text{bb})}$  is provided by  $I_{\text{eff}}^{(\text{bb})} \approx I \cdot \frac{\Gamma}{\Delta\nu_L}$  which yields  $I_{\text{eff}}^{(\text{bb})} \approx 9.6 \cdot 10^{-4} \text{ W cm}^{-2}$ . From these figures the ratio of the photon count rates for broad- and narrowband excitation conditions can be calculated according to Equation (15),

$$\frac{C_{\text{nb}} \left( I_{\text{eff}}^{(\text{nb})} \right)}{C_{\text{bb}} \left( I_{\text{eff}}^{(\text{bb})} \right)} = \frac{D \cdot R_{\infty} \frac{I_{\text{eff}}^{(\text{nb})}}{I_s} \left( 1 + \frac{I_{\text{eff}}^{(\text{nb})}}{I_s} \right)^{-1}}{D \cdot R_{\infty} \frac{I_{\text{eff}}^{(\text{bb})}}{I_s} \left( 1 + \frac{I_{\text{eff}}^{(\text{bb})}}{I_s} \right)^{-1}} = \frac{I_{\text{eff}}^{(\text{nb})} \left( I_s + I_{\text{eff}}^{(\text{bb})} \right)}{I_{\text{eff}}^{(\text{bb})} \left( I_s + I_{\text{eff}}^{(\text{nb})} \right)} = 133 \quad (15)$$

where  $C_{\text{nb}}$  ( $C_{\text{bb}}$ ) corresponds to the photon count rate for narrowband (broadband) excitation at the corresponding effective excitation intensity. The calculated number of 133 is in very good agreement with the ratio  $\frac{195000 \text{ cps}}{1350 \text{ cps}} = 144$  that has been observed experimentally.

## Acknowledgements

We thank Dominique Ernst for assistance with the streak camera experiments. This work was supported financially by the Volkswagen Foundation and the Deutsche Forschungsgemeinschaft (DFG), which is gratefully acknowledged.

**Keywords:** perylene bisimide · photophysics · Shpol'skii matrix · single-molecule spectroscopy · supramolecular chemistry

- [1] V. Balzani, A. Venturi, A. Credi, *Molecular Devices and Machines*, Wiley-VCH, 2003.
- [2] P. F. Barbara, A. J. Gesquiere, S. J. Park, Y. J. Lee, *Acc. Chem. Res.* **2005**, *38*, 602–610.
- [3] F. Schindler, J. M. Lupton, J. Müller, J. Feldmann, U. Scherf, *Nat. Mater.* **2006**, *5*, 141–146.
- [4] O. Mirzov, T. Pullerits, F. Cichos, C. Von Borczyskowski, I. G. Scheblykin, *Chem. Phys. Lett.* **2005**, *408*, 317–321.
- [5] H. Uji-i, S. M. Melnikov, A. Deres, G. Bergamini, F. C. De Schryver, A. Herrmann, K. Müllen, J. Enderlein, J. Hofkens, *Polymer* **2006**, *47*, 2511–2518.
- [6] M. Van der Auweraer, I. Scheblykin, *Chem. Phys.* **2002**, *275*, 285–306.
- [7] A. Pugzlys, R. Augulis, P. H. M. Van Loosdrecht, C. Didruga, V. A. Malyshev, J. Knoester, *J. Phys. Chem. B* **2006**, *110*, 20268–20276.

- [8] E. Lang, A. Sorokin, M. Drechsler, Y. V. Malyukin, J. Köhler, *Nano Lett.* **2005**, *5*, 2635–2640.
- [9] M. Vacha, M. Furuki, L. S. Pu, K. Hashizume, T. Tani, *J. Phys. Chem. B* **2001**, *105*, 12226–12229.
- [10] I. H. M. van Stokkum, B. Gobets, T. Gensch, F. van Mourik, K. J. Hellingwerf, R. van Grondelle, J. T. M. Kennis, *Photochem. Photobiol.* **2006**, *82*, 380–388.
- [11] C. Tietz, F. Jelezko, U. Gerken, S. Schuler, A. Schubert, H. Rogl, J. Wrachtrup, *Biophys. J.* **2001**, *81*, 556–562.
- [12] X. Hu, T. Ritz, A. Damjanovic, F. Autenrieth, K. Schulten, *Q. Rev. Biophys.* **2002**, *35*, 1–62.
- [13] R. J. Cogdell, A. Gall, J. Köhler, *Q. Rev. Biophys.* **2006**, *39*, 227–324.
- [14] J. Psencik, Y. Z. Ma, J. B. Aranello, J. Garcia-Gil, T. Holzwarth, T. Gillbro, *Photosynth. Res.* **2002**, *71*, 5–18.
- [15] L. Schmidt-Mende, A. Fechtenkötter, K. Müllen, E. Moons, R. H. Friend, J. D. MacKenzie, *Science* **2001**, *293*, 1119–1122.
- [16] L. Y. Park, D. G. Hamilton, E. A. McGehee, K. A. McMenimen, *J. Am. Chem. Soc.* **2003**, *125*, 10586–10590.
- [17] F. Würthner, Z. Chen, F. J. M. Hoeben, P. Osswald, C.-C. You, P. Jonkheijm, J. v. Herrikhuysen, A. P. H. J. Schenning, P. P. A. M. van der Schoot, E. W. Meijer, E. H. A. Beckers, S. C. J. Meskers, R. A. J. Janssen, *J. Am. Chem. Soc.* **2004**, *126*, 10611–10618.
- [18] W. Herbst, K. Hunger, *Industrial Organic Pigments: Production, Properties, Applications*, Wiley-VCH, **1997**.
- [19] L. Zang, R. Liu, M. W. Holman, K. T. Nguyen, D. M. Adams, *J. Am. Chem. Soc.* **2002**, *124*, 10640–10641.
- [20] R. Métivier, F. Kulzer, T. Weil, K. Müllen, T. Basché, *J. Am. Chem. Soc.* **2004**, *126*, 14364–14365.
- [21] M. Cotlet, S. Masuo, M. Lor, E. Fron, M. Van der Auweraer, K. Müllen, J. Hofkens, F. C. De Schryver, *Angew. Chem.* **2004**, *116*, 6242–6246; *Angew. Chem. Int. Ed.* **2004**, *43*, 6116–6120.
- [22] F. Würthner, A. Sautter, *Org. Biomol. Chem.* **2003**, *1*, 240–243.
- [23] F. Würthner, C. C. You, C. R. Saha-Möller, *Chem. Soc. Rev.* **2004**, *33*, 133–146.
- [24] A. Sautter, B. K. Kaletas, D. G. Schmid, R. Dobrawa, M. Zimine, G. Jung, I. H. M. van Stokkum, L. De Cola, R. M. Williams, F. Würthner, *J. Am. Chem. Soc.* **2005**, *127*, 6719–6729.
- [25] T. D. M. Bell, A. Stefan, S. Masuo, T. Vosch, M. Lor, M. Cotlet, J. Hofkens, S. Bernhardt, K. Müllen, M. Van der Auweraer, J. W. Verhoeven, F. C. De Schryver, *ChemPhysChem* **2005**, *6*, 942–948.
- [26] R. Métivier, F. Nolde, K. Müllen, T. Basché, *Phys. Rev. Lett.* **2007**, *98*, 047802.
- [27] M. A. Izquierdo, T. D. M. Bell, S. Habuchi, E. Fron, R. Pilot, T. Vosch, S. De Feyter, J. Verhoeven, J. Jacob, K. Müllen, J. Hofkens, F. C. De Schryver, *Chem. Phys. Lett.* **2005**, *401*, 503–508.
- [28] M. Cotlet, S. Masuo, G. Luo, J. Hofkens, M. Van der Auweraer, J. Verhoeven, K. Müllen, X. S. Xie, F. C. De Schryver, *Proc. Natl. Acad. Sci. USA* **2004**, *101*, 14343–14348.
- [29] Ch. Scharf, K. Peter, P. Bauer, Ch. Jung, M. Thelakkat, J. Köhler, *Chem. Phys.* **2006**, *328*, 403–409.
- [30] J. Hofkens, T. Vosch, M. Maus, F. Kohn, M. Cotlet, T. Weil, A. Herrmann, K. Müllen, F. C. De Schryver, *Chem. Phys. Lett.* **2001**, *333*, 255–263.
- [31] P. Osswald, D. Leusser, D. Stalke, F. Würthner, *Angew. Chem.* **2005**, *117*, 254–257; *Angew. Chem. Int. Ed.* **2005**, *44*, 250–253.
- [32] W. E. Ford, P. V. Kamat, *J. Phys. Chem.* **1987**, *91*, 6373–6380.
- [33] G. Seybold, G. Wagenblast, *Dyes Pigm.* **1989**, *11*, 303–317.
- [34] R. Gvishi, R. Reisfeld, Z. Burshtein, *Chem. Phys. Lett.* **1993**, *213*, 338–344.
- [35] C.-C. You, R. Dobrawa, C. R. Saha-Möller, F. Würthner, *Top. Curr. Chem.* **2005**, *258*, 39–82.
- [36] R. A. L. Vallée, M. Cotlet, M. Van der Auweraer, J. Hofkens, K. Müllen, F. C. De Schryver, *J. Am. Chem. Soc.* **2004**, *126*, 2296–2297.
- [37] J. Hernando, J. P. Hoogenboom, E. M. H. P. Van Dijk, J. J. Garcia-Lopez, M. Crego-Calama, D. N. Reinhoudt, N. F. Van Hulst, M. F. Garcia-Parajo, *Phys. Rev. Lett.* **2004**, *93*, 236404.
- [38] F. Würthner, *Pure Appl. Chem.* **2006**, *78*, 2341–2349.
- [39] R. J. Pfab, J. Zimmermann, C. Hettich, I. Gerhardt, A. Renn, V. Sandoghdar, *Chem. Phys. Lett.* **2004**, *387*, 490–495.
- [40] A. C. Wirtz, M. Dokter, C. Hofmann, E. J. J. Groenen, *Chem. Phys. Lett.* **2006**, *417*, 383–388.
- [41] C. Hettich, C. Schmitt, J. Zitzmann, S. Kuhn, I. Gerhardt, V. Sandoghdar, *Science* **2002**, *298*, 385–389.
- [42] J. Michaelis, C. Hettich, J. Mlynek, V. Sandoghdar, *Nature* **2000**, *405*, 325–328.
- [43] Ch. Brunel, B. Lounis, Ph. Tamarat, M. Orrit, *Phys. Rev. Lett.* **1999**, *83*, 2722–2725.
- [44] B. Lounis, W. E. Moerner, *Nature* **2000**, *407*, 491–493.
- [45] P. Tamarat, T. Gäbel, J. R. Rabeau, M. Khan, A. D. Greentree, H. Wilson, L. C. L. Hollenberg, S. Praver, P. Hemmer, F. Jelezko, J. Wrachtrup, *Phys. Rev. Lett.* **2006**, *97*, 083002.
- [46] E. Lang, F. Würthner, J. Köhler, *ChemPhysChem* **2005**, *6*, 935–941.
- [47] E. Lang, F. Würthner, J. Köhler, *ChemPhysChem* **2006**, *7*, 283.
- [48] F. Würthner, A. Sautter, D. Schmid, P. J. A. Weber, *Chem. Eur. J.* **2001**, *7*, 894–902.
- [49] E. V. Shpol'skii, A. A. Il'ina, L. A. Klimova, *Dokl. Akad. Nauk SSSR* **1952**, *87*, 935–938.
- [50] E. Lang, J. Baier, J. Köhler, *J. Microsc.* **2006**, *222*, 118–123.
- [51] W. P. Ambrose, Th. Basché, W. E. Moerner, *J. Chem. Phys.* **1991**, *95*, 7150–7163.
- [52] Y. G. Vainer, M. A. Kol'chenko, A. V. Naumov, R. I. Personov, S. J. Zilker, *J. Lumin.* **2000**, *86*, 265–272.
- [53] M. Orrit, J. Bernard, *Phys. Rev. Lett.* **1990**, *65*, 2716–2719.
- [54] A. J. van Strien, J. Schmidt, *Chem. Phys. Lett.* **1980**, *70*, 513–517.
- [55] R. Brown, J. Wrachtrup, M. Orrit, J. Bernard, C. von Borczyskowski, *J. Chem. Phys.* **1994**, *100*, 7182–7191.
- [56] A. C. J. Brouwer, E. J. J. Groenen, J. Schmidt, *Phys. Rev. Lett.* **1998**, *80*, 3944–3947.
- [57] S. Mais, J. Tittel, Th. Basché, C. Bräuchle, W. Göhde, H. Fuchs, G. Müller, K. Müllen, *J. Phys. Chem. A* **1997**, *101*, 8435–8440.
- [58] A.-M. Boiron, B. Lounis, M. Orrit, *J. Chem. Phys.* **1996**, *105*, 3969–3974.
- [59] J. Bernard, L. Fleury, H. Talon, M. Orrit, *J. Chem. Phys.* **1993**, *98*, 850–859.
- [60] Ph. Tamarat, PhD Thesis, University of Bordeaux, France, **1996**.
- [61] W. Siebrand in *In the Triplet State*, Cambridge University Press, **1967**, p. 31.
- [62] S. Kummer, Th. Basché, C. Bräuchle, *Chem. Phys. Lett.* **1994**, *229*, 309–316.
- [63] F. Jelezko, B. Lounis, M. Orrit, *J. Chem. Phys.* **1997**, *107*, 1692–1702.
- [64] B. R. Henry, W. Siebrand, *J. Chem. Phys.* **1971**, *54*, 1072–1085.
- [65] V. Lawetz, G. Orlandi, W. Siebrand, *J. Chem. Phys.* **1972**, *56*, 4058–4072.
- [66] R. H. Clarke, H. A. Frank, *J. Chem. Phys.* **1976**, *65*, 39–47.
- [67] K. F. Freed, S. H. Lin, *Chem. Phys.* **1975**, *11*, 409–432.
- [68] M. Bixon, J. Jortner, *J. Chem. Phys.* **1968**, *48*, 715–726.

Received: March 13, 2007

Published online on May 25, 2007